Polyhedron 150 (2018) 47–53

Contents lists available at ScienceDirect

Polyhedron

journal homepage: www.elsevier.com/locate/poly

Heptanuclear heterometallic Cu_5Ln_2(Ln = Gd, Tb) complexes: Synthesis, crystal structures, and magnetic properties studies

Despina Dermitzaki, Ourania Bistola, Michael Pissas, Vassilis Psycharis, Yiannis Sanakis, Catherine P. Raptopoulou *

Institute of Nanoscience and Nanotechnology, NCSR "Demokritos", 15310 Aghia Paraskevi, Athens, Greece

ARTICLE INFO

Article history:
Received 29 March 2018
Accepted 2 May 2018
Available online 9 May 2018

This work is dedicated to our dearest friend, colleague Prof. Spyros P. Perlepes on the occasion of his 65th birthday.

Keywords:
Copper(II)–Lanthanide(III) complexes
Crystal structures
Magnetic measurements
Magnetocaloric effect
Single-molecule magnet

ABSTRACT

The reaction of $Ln(NO_3)_3{\cdot}6H_2O$ (Ln = Gd, Tb) and $Cu(O_2CMe)_2{\cdot}H_2O$ with the polydentate Schiff base ligand $OH{-}C_{10}H_7{-}CH{=}NC(C_2H_5)(CH_2OH)_2$ (H_3L) in Me_2CO afforded the heptanuclear heterometallic complexes $[Cu_5Ln_2(O_2CMe)_2(NO_3)_4(L)_2(HL)_2]$ (Ln = Gd (**1**), Tb (**2**)) which were characterized by single-crystal X-ray crystallography (**1**) and powder XRD measurements (**2**). Both complexes are isomorphous and consist of a central core $\{Cu^{II}_5Ln^{III}_2(\mu_3\text{-OR})_6(\mu_3\text{-}O_2CMe)_2\}^{8+}$ described as two distorted centrosymmetrically related cubane subunits, $\{Cu^{II}_3Ln^{III}(\mu_3\text{-OR})_3(\mu_3\text{-}O_2CMe)\}^{5+}$, with the common apex, Cu(1), residing on an inversion center. Peripheral ligation and bridging is provided by two triply and two doubly deprotonated Schiff base ligands, two μ_3-acetates and four chelate nitrates. Magnetic susceptibility measurements revealed the presence of dominant ferromagnetic interactions for both complexes. The magnetocaloric effect of **1** was examined via isothermal magnetization measurements under various applied fields and the maximum entropy change was found equal to 15.7 J kg^{-1} K^{-1} at 2 K for ΔH = 5 T. Ac susceptibility measurements of **2** revealed slow magnetic relaxation process suggesting the presence of single-molecule magnet behavior.

1. Introduction

Molecular magnetic materials with interesting structures and noteworthy physical properties have been extensively studied over the past decades, and have been proposed for potential applications in high-density information storage devices, quantum computing, spintronics and magnetic refrigeration [1]. The useful physical property of each material, depends on the potential application. For example, molecular magnetic materials should exhibit large energy barrier for magnetization reversal in order to find potential applications as information storage media. The combination of 3d/4f metal ions in one molecule can result in high spin ground states (via the involvement of the 3d metal ions) along with large single-ion anisotropy (via the presence of the 4f metal ions) and provides, in many cases, considerable energy barriers for magnetization reversal leading to single-molecule magnet (SMM) behavior. On the contrary, magnetic refrigeration requires molecules possessing a large spin ground state and negligible magnetic anisotropy. The magnetic refrigeration is based on the magnetocaloric effect (MCE) i.e. the isothermal change of magnetic entropy (ΔS_m) and adiabatic change of temperature (ΔT_{ad}) that follow a change of the applied magnetic field (ΔH).The refrigeration cycle involves (i) the adiabatic magnetization of the sample, i.e. the increase of the external magnetic field followed by the decrease of the magnetic entropy and heat capacity and increase of the temperature, (ii) the isomagnetic enthalpic transfer, i.e. the removal of the added heat from the sample under constant magnetic field, (iii) the adiabatic demagnetization of the sample, i.e. the decrease of the external magnetic field followed by cooling of the sample because the magnetic entropy remains constant, and (iv) the isomagnetic entropic transfer, i.e. the sample is cooler than the environment therefore it is heated again in order for a new cycle to begin. The upper limit for the entropy change at $T = \infty$ is $\Delta S_m = R\ln(2S + 1)$, where R is the gas constant and S is the spin value. In order to exhibit large MCE with potential applications as low-temperature magnetic refrigerants, the molecular magnetic materials should combine a large spin ground state, negligible magnetic anisotropy, considerable degeneracy via low-lying excited states, large metal-to-ligand ratio and low molecular weight. Molecules with high spin ground state and large anisotropy, such as Mn_{12} and Fe_8, have been initially examined as potential magnetic refrigerants in the liquid helium regime, albeit the fact that the magnetic anisotropy reduces the maxima of the magnetic entropy due to degeneracy lifting of the energy levels [2]. The use of the isotropic Gd^{III} (S = 7/2) ion has contributed in both

* Corresponding author. Fax: +30 210 6519430.
E-mail address: c.raptopoulou@inn.demokritos.gr (C.P. Raptopoulou).

https://doi.org/10.1016/j.poly.2018.05.003
0277-5387/

research fields, i.e. single-molecule magnets and magnetic refrigerants. Gd-based complexes and multi-dimensional coordination polymers have been extensively studied as magnetic refrigerants with entropy change $-\Delta S_m$ up to 59 J kg^{-1} K^{-1} (at 3 K and ΔH = 7 T) [3–8].

The synthesis of heterometallic 3d/4f complexes is mainly based on the *hard and soft acids and bases* (HSAB) principle according to which, ligands possessing different donor atoms suitable for coordination to 3d and 4f metal ions, preferably nitrogen and oxygen, respectively, are used. Suitable co-ligands may also be present in order to assist the self-assembly processes. In general, the mixing of 3d and 4f ions with organic ligands would produce pure 3d or 4f complexes rather than heterometallic 3d/4f ones. The final products of the reactions depend on their relative potential energy and based on HSAB rules it is assumed that the use of suitably designed organic ligands which contain one or more coordination pockets of both nitrogen and oxygen donors would favor the synthesis of 3d/4f heterometallic complexes. Among the ligands used, Schiff bases have been widely used for the synthesis of 3d, 4f and 3d/4f complexes because they offer the advantage of modular synthesis via various combinations of starting materials and in addition they can be easily functionalized by choosing starting materials with the desired side groups [9–12]. The various Schiff base ligands containing coordination pockets as well as hydroxyl, amino and carboxylate groups have resulted in a large number of 3d/4f complexes [13–22]. Among them, Cu^{II}-Ln^{III} Schiff base complexes have been extensively studied, for example dinuclear [23], trinuclear [24–27], tetranuclear [28–31] and higher nuclearity clusters [17,32–34]. Neighboring Ln^{III} ions exhibit similar ionic radius and coordinating features, leading to isomorphic complexes of the whole 4f series, whose magnetic properties are governed by the nature of the f orbitals. The significant magnetic anisotropy of Tb^{III}, Dy^{III}, Ho^{III} and Er^{III}, as a result of the large spin–orbital coupling as well as the crystal-field effect, make these ions excellent candidates for the synthesis of molecular nanomagnets, whereas the isotropic Gd^{III} ion is more suitable for magnetocaloric measurements and more importantly as a model ion for theoretical calculations concerning exchange interactions within 3d/4f clusters.

We present herein a part of our work on the Cu^{II}/Ln^{III} chemistry with Schiff base ligands based on 2-hydroxy-1-naphthaldehyde and various amino-alcohols as a means to new molecular magnetic materials, i.e. the synthesis and magnetic study of the heptanuclear clusters $[Cu_5Ln_2(O_2CMe)_2(NO_3)_4(L)_2(HL)_2]$ (Ln = Gd (**1**), Tb (**2**), and H_3L = OH—$C_{10}H_7$—CH=NC(C_2H_5)(CH_2OH)$_2$).

2. Experimental

2.1. General and spectroscopic measurements

All manipulations were performed under aerobic conditions using materials as received (Aldrich Co). All chemicals and solvents were of reagent grade. The ligand OH—$C_{10}H_7$—CH=NC(C_2H_5)(CH_2-OH)$_2$, H_3L was synthesized by the equimolar reaction of 2-hydroxy-1-naphthaldehyde and 2-amino-2-ethyl-1,3-propanediol in MeOH. The immediately formed yellow solution was refluxed for 1 h and concentrated in rotary evaporator to obtain yellow crystals of H_3L. Elemental analysis for carbon, hydrogen, and nitrogen was performed on a Perkin Elmer 2400/*II* automatic analyzer. Infrared spectra were recorded as KBr pellets in the range 4000–400 cm^{-1} on a Bruker Equinox 55/S FT-IR spectrophotometer. Variable-temperature and field magnetic measurements were carried out on polycrystalline samples using Quantum Design PPMS 9T and SQUID magnetometer Quantum Design MPMS 5.5. Diamagnetic corrections were estimated from Pascal's constants.

2.2. Compound preparations

2.2.1. $[Cu_5Gd_2(O_2CMe)_2(NO_3)_4(L)_2(HL)_2]\cdot 4Me_2CO$ (1·4Me$_2$CO)

Solid Gd(NO_3)$_3$·6H_2O (0.075 mmol, 0.0339 g) was added under stirring to a yellow solution of H_3L (0.10 mmol, 0.0273 g) in Me_2CO (15 mL). After 10 min of stirring, solid Cu(O_2CMe)$_2$·H_2O (0.10 mmol, 0.0200 g) was added and the solution became dark green. The stirring continued for 30 min and the final reaction solution was kept in closed vials. Crystals of **1** were formed after three days. Yield: 0.0095 g, ~20% based on Cu^{II}. $C_{80}H_{96}N_8O_{32}Cu_5Gd_2$ (f.w. = 2313.84) requires C, 41.52; H, 4.18; N, 4.84%. Found: C, 41.39; H, 4.15; N, 4.82%. FT-IR (KBr pellets, cm^{-1}): 3376(br), 3058(w), 2964(m), 2924(m), 1703(m), 1688(m), 1620(vs), 1605(vs), 1585(s), 1583(s), 1538(s), 1506(s), 1454(s), 1429(s), 1381(vs), 1362(s), 1336(s), 1292(s), 1275(sh), 1250(m), 1218(w), 1188(s), 1160(s), 1140(s), 1119(m), 1088(m), 1065(m), 1032(s), 998(m), 972(w), 948(m), 935(w), 912(m), 859(m), 830(s), 816(m), 780(m), 745(s), 659(w), 645(s), 575(s), 528(w), 514(w), 488(m), 463(m), 450(m), 415(m).

2.2.2. $[Cu_5Tb_2(O_2CMe)_2(NO_3)_4(L)_2(HL)_2]\cdot 4Me_2CO$ (2·4Me$_2$CO)

Solid Tb(NO_3)$_3$·6H_2O (0.075 mmol, 0.0340 g) was added under stirring to a yellow solution of H_3L (0.075 mmol, 0.0205 g) in Me_2-CO (5 mL). After 10 min of stirring, solid Cu(O_2CMe)$_2$·H_2O (0.075 mmol, 0.0150 g) was added and the solution became dark green. The stirring continued for 30 min and the final reaction solution was kept in closed vials. Microcrystalline **2** was formed after five days. The identity of the microcrystalline material was established by powder XRD measurements (see Fig. S1). Yield: 0.0219 g, ~60% based on Cu^{II}. $C_{80}H_{96}N_8O_{32}Cu_5Tb_2$ (f.w. = 2317.26) requires C, 41.47; H, 4.18; N, 4.84%. Found: C, 41.37; H, 4.16; N, 4.82%. FT-IR (KBr pellets, cm^{-1}): 3378(br), 3058(w), 2965(m), 2924(m), 1704 (m), 1689(m), 1620(vs), 1604(vs), 1586(s), 1583(s), 1538(s), 1505 (s), 1454(s), 1428(s), 1381(vs), 1362(s), 1337(s), 1292(s), 1276 (sh), 1250(m), 1219(w), 1188(s), 1161(s), 1140(s), 1119(m), 1089 (m), 1065(m), 1032(s), 998(m), 970(w), 948(m), 936(w), 912(m), 858(m), 830(s), 817(m), 780(m), 746(s), 659(w), 645(s), 576(s), 528(w), 514(w), 487(m), 463(m), 451(m), 414(m).

2.3. Single crystal X-ray crystallography

Crystals of **1**·4Me_2CO (0.12 × 0.15 × 0.30 mm) were taken from the mother liquor and immediately cooled to −103 °C. Diffraction measurements were made on a Rigaku R-AXIS SPIDER Image Plate diffractometer using graphite monochromated Mo Kα radiation. Data collection (ω-scans) and processing (cell refinement, data reduction and Empirical absorption correction) were performed using the CrystalClear program package [35]. The structure was solved by direct methods using SHELXS-97 and refined by full-matrix least-squares techniques on F^2 with SHELXL ver2014/6 [36]. Important crystallographic and refinement data are listed in Table 1. Further experimental crystallographic details for **1**·4Me_2CO: $2\theta_{max}$ = 54°; reflections collected/unique/used, 53464/9632 [R_{int} = 0.0283]/9632; 742 parameters refined; $(\Delta/\sigma)_{max}$ = 0.002; $(\Delta\rho)_{max}/(\Delta\rho)_{min}$ = 0.497/−0.381 e/Å^3; *R*1/w*R*2 (for all data), 0.0447/0.0220. Hydrogen atoms were either located by difference maps and were refined isotropically or were introduced at calculated positions as riding on bonded atoms. All non-hydrogen atoms were refined anisotropically. Plots of the structures were drawn using the Diamond 3 program package [37].

3. Results and discussion

3.1. Synthesis and spectroscopic characterization

The reaction between Ln(NO_3)$_3$·xH_2O (Ln = Gd, Tb) and Cu(O_2-CMe)$_2$·H_2O with the Schiff base ligand H_3L in Me_2CO under stirring

Table 1
Crystallographic data for **1**·4Me_2CO.

	1·4Me_2CO
Formula	$C_{80}H_{96}Cu_5Gd_2N_8O_{32}$
Fw	2313.84
Space group	$P2_1/c$
a (Å)	12.9395(15)
b (Å)	18.8940(19)
c (Å)	18.6340(20)
α (°)	90.0
β (°)	103.850(4)
γ (°)	90.0
V (Å^3)	4423.0(8)
Z	2
T (°C)	−103
Radiation	Mo Kα 0.71073
ρ_{calcd} (g cm^{-3})	1.737
μ (mm^{-1})	2.744
Reflections with $I > 2\sigma(I)$	8844
R_1[a]	0.0189
wR_2[a]	0.0437

$R_1 = \Sigma(|F_o| - |F_c|)/\Sigma(|F_o|)$ and $wR_2 = \{\Sigma[w(Fo^2\text{-}Fc^2)^2]/\Sigma[w(F_o^2)^2]\}^{1/2}$.
[a] $w = 1/[\sigma^2(F_o^2) + (\alpha P)^2 + bP]$ and $P = (\max F_o^2, 0) + 2F_c^2)/3$, $a = 0.0183$ and $b = 2.8767$.

at room temperature afforded dark green solutions which gave green crystals (**1**) or green microcrystalline materials (**2**) from closed vials, according to the reaction:

$$2Ln(NO_3)_3\cdot 6H_2O + 5Cu(O_2CMe)_2\cdot H_2O + 4H_3L \xrightarrow{Me_2CO} \times [Cu_5Ln_2(O_2CMe)_2(NO_3)_4(L)_2(HL)_2]_{\mathbf{1-2}} + 2HNO_3 + 8MeCO_2H + 17H_2O \quad (1)$$

The above reaction performed in different solvents (MeOH, MeCN etc) and also similar reactions involving other copper salts, e.g. chlorides, nitrates, perchlorates, gave microcrystalline or oily products which could not be identified.

The IR spectrum of **1**–**2** exhibits a broad band a 3378 cm^{-1} attributed to the ν(OH) vibrations due to the presence of the alkoxo groups of the HL^- ligands. The bands at 3060, 2960 and 2920 cm^{-1} are attributed to the ν(=CH), ν(CH_3) and ν(CH_2) stretching vibrations of the Schiff base and acetate ligands. A set of peaks in the 1600–1400 cm^{-1} region are attributed to the stretching vibrations of the α-substituted naphthalene ring and the strong band at ~745 cm^{-1} is attributed to the out-of-plane CH deformation vibrations of the naphthalene ring. The very strong band at ~1605 cm^{-1} is due to ν(C=N) vibration of the Schiff base ligands. This band appears at lower frequency with respect to H_3L (1620 cm^{-1}) suggesting coordination of the metal ions through the imino nitrogen. The ν(C—O) stretching frequency of the phenolic oxygen of H_3L is seen at 1396 cm^{-1} and shifts to ~1355 cm^{-1} indicating coordination to the metal ions [38]. The medium intensity bands at ~1703 cm^{-1} are attributed to the ν(C=O) vibration of the solvate Me_2CO molecules. The strong absorption bands at 1250 and 1360 cm^{-1} are attributed to the symmetric and antisymmetric vibrations of the coordinated nitrates [39]. The ν_{as}(C=O) and ν_s(C=O) are observed at ~1505 and ~1362 cm^{-1}, respectively, with Δ ~143 cm^{-1} as expected for the bridging mode of the acetate ligands. The strong band at ~1380 cm^{-1} is attributed to the presence of $\nu_3(E')$ [ν_d(NO)] mode of uncoordinated D_{3h} ionic nitrates; their presence is probably due to partial substitution of coordinated nitrates from bromides during the preparation of the KBr pellet under pressure [40].

3.2. Description of the structure

Complex**1** crystallizes in the monoclinic space group $P2_1/c$; complex **2** is isomorphous to **1** based on powder XRD data (Fig. S1). The asymmetric unit of **1** contains half of the complex and two acetone solvates. The complex is neutral and consists of

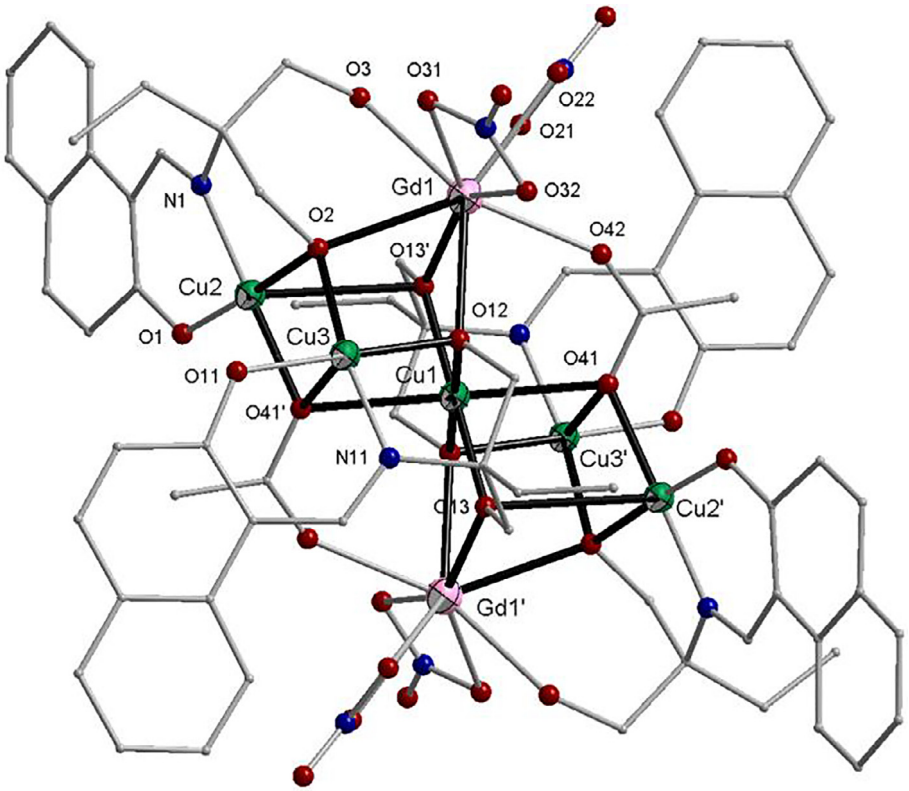

Fig. 1. Partially labeled plot of **1**.The metal core is highlighted in black. Color code: Gd pink octant, Cu green octant, O red, N blue, C light grey. Primed atoms are generated by symmetry: (′) −*x*, 1 − *y*, 2 − *z*. (Colour online.)

five Cu^{II} and two Gd^{III} ions which are held together via six μ_3-O_{alkoxo} and two μ_3-$O_{acetato}$ atoms. The topology of the central core, $\{Cu^{II}_5Gd^{III}_2(\mu_3\text{-}OR)_6(\mu_3\text{-}O_2CMe)_2\}^{8+}$, is described as two distorted cubane subunits, $\{Cu^{II}_3Gd^{III}(\mu_3\text{-}OR)_3(\mu_3\text{-}O_2CMe)\}^{5+}$, with a common apex on Cu(1) which resides on an inversion center. The molecular structure of the heptanuclear complex $[Cu_5Gd_2(O_2CMe)_2(NO_3)_4(L)_2(\text{-}HL)_2]$ (**1**) is shown in Fig. 1. Selected bond distances and angles are listed in Table 2.

The seven metal ions are held together via two L^{3-} and two HL^{2-} ligands and two μ_3-κ^3O:$\kappa O'$ $MeCO_2^-$ ligands. The triply deprotonated ligands, L^{3-}, behave as μ_5-κ^3O,κ^3O',$\kappa O''$,κN (Scheme 1) and bridge atoms Cu(1)/Cu(3)/Gd(1) of one cubane subunit with atoms Cu(2′)/Gd(1′) of its centrosymmetric congener. The L^{3-} ligand (defined by atoms O(11)/N(11)/O(12)/O(13)) chelates around Cu(3) through the $O_{phenoxo}$ (O(11)), N_{imino} (N(11)) and O_{alkoxo} (O(12)) atoms; the latter is also coordinated to Gd(1) and Cu(1), thus acting as μ_3-bridge. The second deprotonated O_{alkoxo} (O(13)) of L^{3-} ligand coordinates to Cu(1) and also to the centrosymmetric Cu(2′) and Gd(1′), acting also as μ_3-bridge. The doubly deprotonated ligands, HL^{2-}, behave as μ_3-κ^3O,$\kappa O'$,$\kappa O''$,κN (Scheme 1) between atoms Cu(2)/Cu(3)/Gd(1) of each cubane subunit. The HL^{2-} ligand (defined by O(1)/N(1)/O(2)/O(3)) chelates around Cu(2) through the $O_{phenoxo}$ (O(1)), N_{imino} (N(1)) and O_{alkoxo} (O(2)) atoms; the latter is also coordinated to Gd(1) and Cu(3), thus acting as μ_3-bridge. The protonated O_{alkoxo}, O(3), is coordinated to Gd(1).

Cu(1) presents distorted octahedral coordination geometry consisting of two deprotonated O_{alkoxo} atoms from two L^{3-} ligands (O(12)/O(13) and their centrosymmetric ones) with Cu(1)-O_{alkoxo} ~1.95 and 1.99 Å in the equatorial plane, and two μ_3-acetato oxygen atoms (O(41)/O(41′)) in the apical positions with Cu(1)-$O_{acetato}$ ~2.46 Å. Cu(2) and Cu(3) and their centrosymmetric ones are five-coordinate with square pyramidal geometry. The equatorial plane in Cu(2) is defined by atoms O(1)/N(1)/O(2) of one HL^{2-} and O(41′) of one μ_3-$O_{acetate}$ with bond distances in the range 1.88–2.02 Å and the apical position is occupied by O(13′) of one L^{3-} at ~2.88 Å. The trigonality index $\tau = 0.02$ indicates almost ideal square pyramidal geometry in Cu(2). The equatorial plane in Cu(3) is defined by atoms O(11)/N(11)/O(12) of one L^{3-} and O(2), one of μ_3-O_{alkoxo} atoms of HL^{2-} with bond distances in the range 1.88–1.97 Å and the apical position is occupied by the μ_3-$O_{acetato}$ atom O(41′) at ~2.49 Å. The trigonality index $\tau = 0.16$ suggests square pyramidal geometry in Cu(3). The coordination sphere around Gd^{III} ions consists of nine oxygen atoms, the μ_3-O_{alkoxo} O(2) and the protonated O_{alkoxo} O(3) of HL^{2-}, the two μ_3-O_{alkoxo} O(12) and O(13) of L^{3-}, the monodentate $O_{acetato}$ O(42) and atoms O(21)/O(22) and O(31)/O(32) from two chelate NO_3^- ions. The bond distances around the gadolinium ions are in the range 2.282(1)–2.565(1) Å. Continuous Shape Measures by using the program SHAPE [41] show that the best-fit polyhedron around the Gd(1) atoms in **1** is either a spherical capped square antiprism CSAPR-9 (CShM = 1.31428) or a muffin MFF-9 (CShM = 1.31490).

The protonated alkoxo group of each HL^{2-} participates in hydrogen bond with one of the Me_2CO solvate molecules [O(3)···O(51) = 2.676 Å (−*x*, 0.5 + *y*, 1.5 − *z*), HO(3)···O(51) = 1.989 Å, O(3)–HO(3)···O(51) = 166.3°; Fig. S2].

Table 2
Selected bond distances (Å) and angles (°) in **1**·4Me_2CO.

Distances			
Gd(1)-O(13′)	2.282(1)	Cu(1)-O(41)	2.460(1)
Gd(1)-O(42)	2.384(1)	Cu(2)-O(1)	1.884(1)
Gd(1)-O(3)	2.420(1)	Cu(2)-N(1)	1.912(2)
Gd(1)-O(12)	2.422(1)	Cu(2)-O(41′)	1.984(1)
Gd(1)-O(22)	2.456(2)	Cu(2)-O(2)	2.016(1)
Gd(1)-O(32)	2.466(2)	Cu(2)-O(13′)	2.878(1)
Gd(1)-O(21)	2.475(2)	Cu(3)-O(11)	1.880(1)
Gd(1)-O(31)	2.516(2)	Cu(3)-N(11)	1.902(2)
Gd(1)-O(2)	2.565(1)	Cu(3)-O(2)	1.957(1)
Cu(1)-O(13)	1.951(1)	Cu(3)-O(12)	1.971(1)
Cu(1)-O(12)	1.994(1)	Cu(3)-O(41′)	2.492(1)
Cu(1)···Cu(2)	3.622(1)	Gd(1)···Cu(1)	3.3131(1)
Cu(1)···Cu(3)	3.129(1)	Gd(1)···Cu(2)	3.845(1)
Cu(2)···Cu(3)	3.001(1)	Gd(1)···Cu(3)	3.529(1)
Angles			
O(13′)-Gd(1)-O(31)	149.8(1)	O(42)-Gd(1)-O(31)	125.2(1)
O(42)-Gd(1)-O(3)	144.8(1)	O(3)-Gd(1)-O(32)	123.1(1)
O(22)-Gd(1)-O(2)	144.2(1)	O(22)-Gd(1)-O(21)	52.1(1)
O(13′)-Gd(1)-O(32)	143.4(1)	O(32)-Gd(1)-O(31)	51.1(1)
O(12)-Gd(1)-O(22)	141.9(1)	O(13′)-Cu(1)-O(12)	86.1(1)
O(42)-Gd(1)-O(2)	138.3(1)	O(13′)-Cu(1)-O(41)	97.8(1)
O(12)-Gd(1)-O(21)	136.5(1)	O(12)-Cu(1)-O(41)	91.8(1)
O(3)-Gd(1)-O(12)	133.9(1)	N(1)-Cu(2)-O(41′)	176.0(1)
O(21)-Gd(1)-O(2)	133.8(1)	O(1)-Cu(2)-O(2)	177.0(1)
O(13′)-Gd(1)-O(22)	130.0(1)	N(11)-Cu(3)-O(2)	169.7(1)
O(32)-Gd(1)-O(21)	125.9(1)	O(11)-Cu(3)-O(12)	179.2(1)
Cu(3)-O(2)-Cu(2)	98.1(1)	Cu(1)-O(13′)-Cu(2)	95.3(1)
Cu(3)-O(2)-Gd(1)	101.7(1)	Cu(1)-O(13′)-Gd(1)	102.7(1)
Cu(2)-O(2)-Gd(1)	113.6(1)	Cu(2)-O(13′)-Gd(1)	95.7(1)
Cu(3)-O(12)-Cu(1)	104.2(1)	Cu(1)-O(41′)-Cu(2)	108.7(1)
Cu(3)-O(12)-Gd(1)	106.4(1)	Cu(1)-O(41′)-Cu(3)	78.4(1)
Cu(1)-O(12)-Gd(1)	96.8(1)	Cu(2)-O(41′)-Cu(3)	83.4(1)

Symmetry operation: (′) −*x*, 1 − *y*, 2 − *z*.

3.3. Magnetic measurements

Magnetic susceptibility measurements as a function of temperature were recorded from polycrystalline samples of **1**–**2** at 1000 Oe dc field. The $\chi_M T$ product for **1** at 300 K is 15.16 cm^3 $Kmol^{-1}$ which is lower than the theoretical value of 17.625 cm^3 $Kmol^{-1}$ for five Cu^{II} ions ($S = 1/2$ with $C = 0.375$ cm^3 $Kmol^{-1}$, $g = 2$) and two Gd^{III} ions ($S = 7/2$ with $C = 7.875$ cm^3 $Kmol^{-1}$, $g = 2$). The $\chi_M T$ product increases gradually as the temperature is decreasing reaching the value of 18.06 cm^3 $Kmol^{-1}$ at 15 K and then it increases rapidly to the value of 24.27 cm^3 $Kmol^{-1}$ at 2 K (Fig. 2). The overall temperature dependence of the $\chi_M T$ product suggests

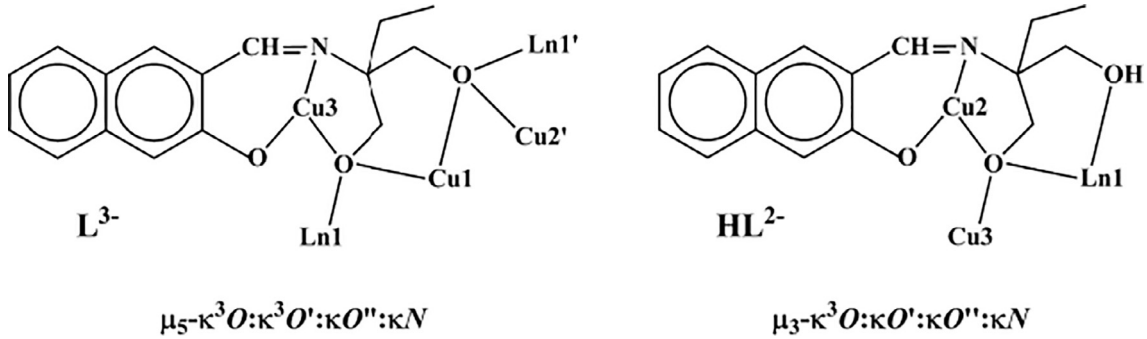

μ_5-κ^3O:κ^3O':$\kappa O''$:κN μ_3-κ^3O:$\kappa O'$:$\kappa O''$:κN

Scheme 1. The coordination modes of the L^{3-} and HL^{2-} ligands in **1**.

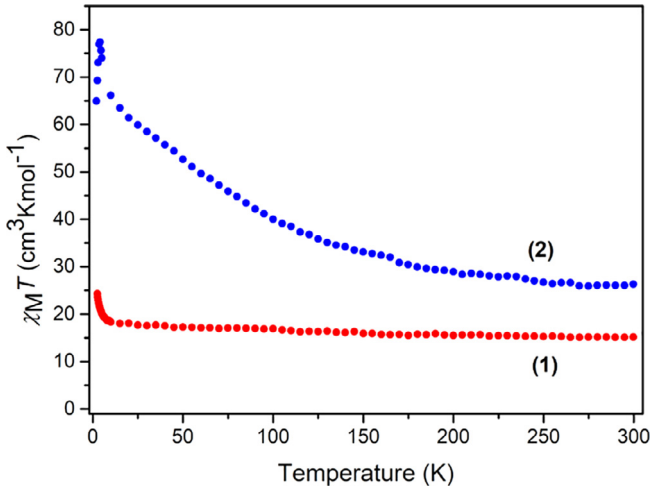

Fig. 2. $\chi_M T$ *vs. T* plots for **1** and **2** at 1000 Oe.

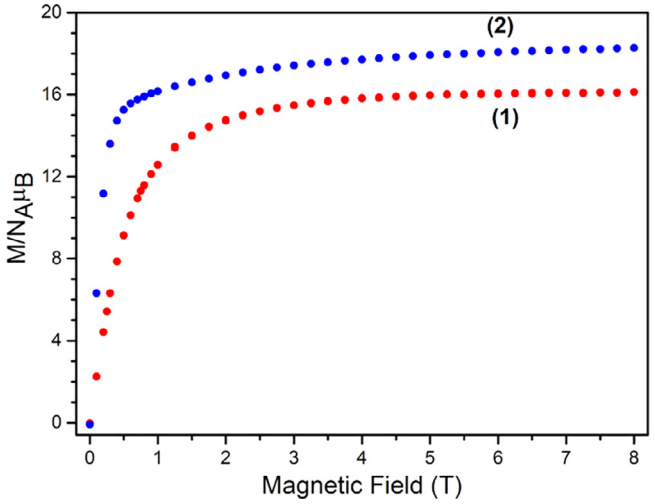

Fig. 3. Magnetization curves for **1** and **2** at 2 K.

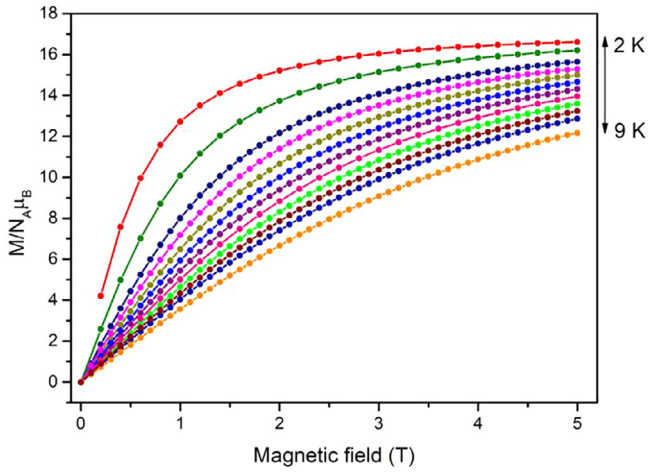

Fig. 4. Field-dependent magnetization plots for **1** at 2–9 K.

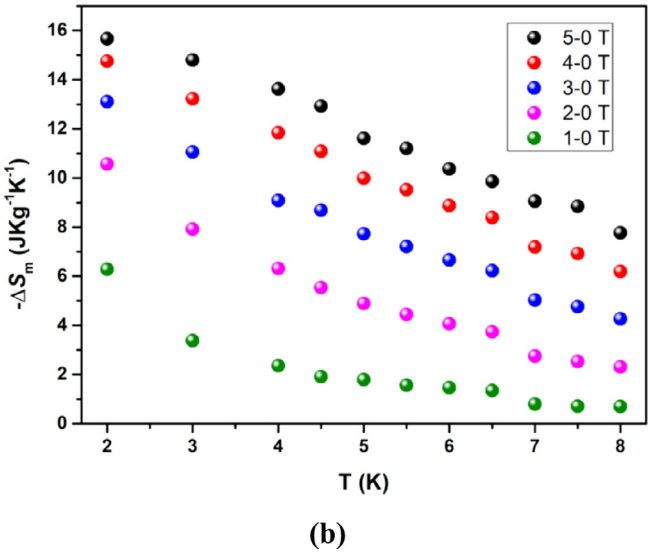

Fig. 5. The temperature dependent magnetic entropy change for **1**.

the presence of dominant ferromagnetic interactions between the five Cu^{II} and the two Gd^{III} ions. The magnetization measurements at 2 K as a function of the external applied field show a rapid increase upon increasing of the magnetic field reaching a value of 16.12 $N\mu_B$ at 8 T (Fig. 3). The clear saturation above 4 T suggests the presence of an isolated ground state of low magnetic anisotropy. The saturation of M at 16.12 μ_B is lower than the value of 19 μ_B expected for two Gd^{III} ($S = 7/2$) ions and five Cu^{II} ($S = 1/2$) ions which are uncoupled or completely ferromagnetically coupled ($S_T = 19/2$), suggesting that some of the metal ions are antiferromagnetically coupled. This can be achieved if we assume that the central Cu^{II} ion has opposite spin arrangement with respect to the other metal ions, leading to a total ground spin state of $S = 17/2$. The saturation value of the magnetization should be then equal to 17 μ_B which is close to the experimental value of 16.12 μ_B.

Magnetization data were recorded in the 2–9 K temperature range under external applied magnetic field up to 5 T in order to explore the magnetic entropy changes $-\Delta S_m$ and evaluate the magnetocaloric effect (MCE) of **1**. Field-dependent magnetization plots for **1** are shown in Fig. 4. The $-\Delta S_m$ can be calculated from the experimental magnetization data by using the Maxwell equation

$$-\Delta S_m(T)_{\Delta H} = \int [\vartheta M(T,H)/\vartheta T]_H dH \quad (2)$$

or by using the simpler numerical approximation to the above integral [42]

$$|\Delta S_m| = \sum_i \frac{M_i - M_{1+1}}{T_i - T_{1+1}} \Delta H_i \quad (3)$$

where M_i and M_{i+1} are the experimental values of magnetization at T_i and T_{i+1} temperatures, respectively, under an applied field of intensity H_i. The experimental values of the magnetic entropy change obtained from the experimental isothermal magnetization curves under various magnetic field variations are shown in Fig. 5. The maximum entropy change of 15.7 J kg^{-1} K^{-1} is obtained at 2 K for $\Delta H = 5$ T. For a system containing two Gd^{III} ($S = 7/2$) and five Cu^{II} ($S = 1/2$) ions which are fully decoupled, the maximum $-\Delta S_m$ value of 27.4 J kg^{-1} K^{-1} can be calculated from the equation $-\Delta S_m = nR\ln(2S + 1)$, which is larger than the value calculated experimentally by isothermal magnetization measurements. The maximum entropy change obtained in several Cu-Gd complexes of various

nuclearities and metal topologies are in the range 11.9–34.5 J kg^{-1} K^{-1} in the temperature range 2.0–4.5 K for ΔH = 7 T [43–47].

The $\chi_M T$ product for **2** at 300 K is 26.32 cm^3 $Kmol^{-1}$ which is slightly larger than the theoretical value of 25.50 cm^3 $Kmol^{-1}$ for five Cu^{II} ions (S = 1/2 with C = 0.375 cm^3 $Kmol^{-1}$, g = 2) and two Tb^{III} ions (S = 3, L = 3, J = 6 with C = 11.81 cm^3 $Kmol^{-1}$, g = 3/2). The $\chi_M T$ product increases gradually upon lowering the temperature and reaches the value of 77.36 cm^3 $Kmol^{-1}$ at 4 K and then drops to 64.95 cm^3 $Kmol^{-1}$ at 2 K (Fig. 2). The overall temperature dependence of the $\chi_M T$ product suggests the presence of dominant ferromagnetic interactions between the five Cu^{II} and the two Tb^{III} ions. The large value of $\chi_M T$ product at 2 K suggests the presence of a large spin ground state. The magnetization measurements at 2 K as a function of the external applied field show a rapid increase upon increasing of the magnetic field reaching a value of 18.28 $N\mu_B$ at 8 T (Fig. 3) without saturation. The value of the magnetization is lower than the value of 23 μ_B expected for two Tb^{III} (J = 6, g = 3/2) ions and five Cu^{II} (S = 1/2, g = 2) ions which are uncoupled or completely ferromagnetically coupled. This behavior indicates the presence of magnetic anisotropy and/or possibly low-lying excited states.

The dynamic magnetic properties of **2** were investigated by ac magnetic susceptibility measurements as a function of temperature at different frequencies and were performed at zero dc field and also under external field of 1000 Oe. The plots of in-phase and out-of-phase ac magnetic susceptibilities at low temperatures under zero dc field are shown in Fig. 6. The data show that the out-of-phase magnetic susceptibility deviates from zero at temperatures below 3 K and at the highest frequencies recorded. The deviation in the values of χ'' is frequency dependent and the tails shown are characteristic of slow relaxation of the magnetization. No maximum in χ'' is observed down to 2 K, which is the lowest temperature for our setup. Application of a dc field of 1000 Oe did not alter the ac signal profile (Fig. S3). If we assume that the relaxation of the magnetization occurs through a single process, the ac susceptibility data can be approximated with the Debye model with $\ln(\chi''/\chi') = \ln(\omega\tau_0) + U_{eff}/k_BT$ ($\omega = 2\pi\nu$) [48] and hence the energy barrier U_{eff}/k_B and τ_0 values can be estimated. The linear fit to the $\ln(\chi''/\chi')$ *versus* 1/T data gave U_{eff}/k_B = 9.4 ± 0.1 K and pre-exponential factor $\tau_0 = 1.1 \pm 0.2 \times 10^{-7}$ s for **2** (Fig. 7). The plot of χ'' *versus* χ' (Cole–Cole plot) for **2** in the temperature range 2.1–3 K at zero dc field is shown in Fig. 8. The data were simulated according to equation

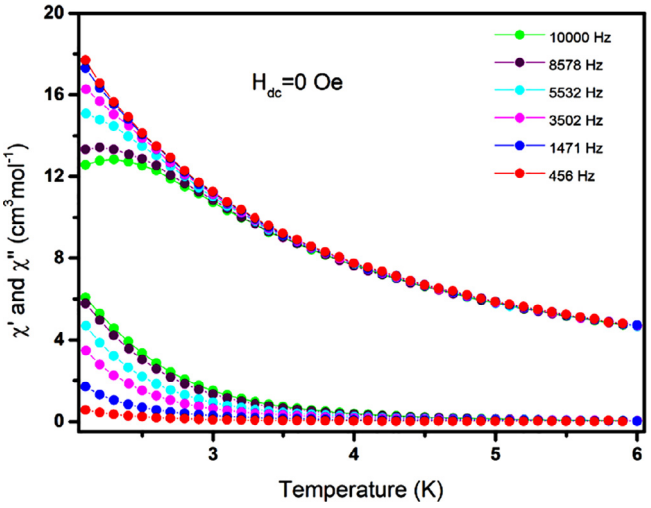

Fig. 6. Temperature dependence of χ' and χ'' of **2** under different frequencies at zero external field.

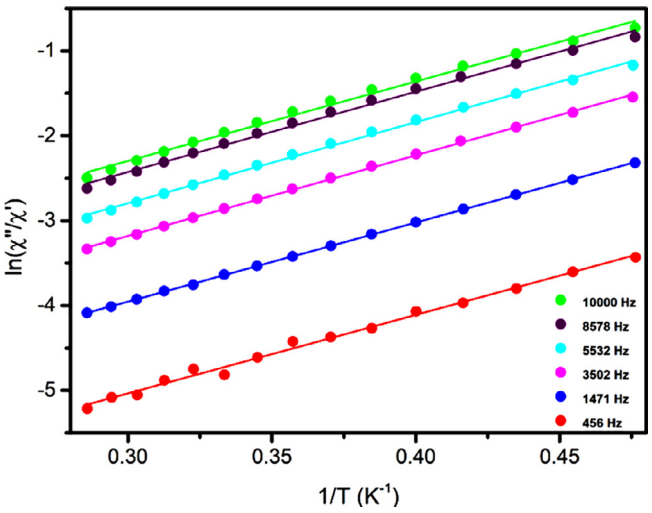

Fig. 7. $\ln(\chi''/\chi')$ *vs.* 1/T plots for **2** in the temperature range 2–3.5 K at various frequencies. The solid lines represent the fitting results over the temperature range.

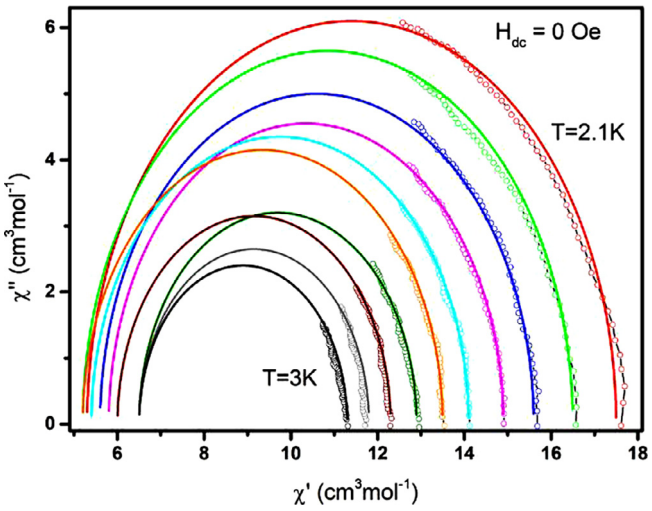

Fig. 8. χ'' *vs.* χ' plots for **2** at zero external field. The solid lines represent the simulation semicircles according to Eq. (4).

$$\chi'' = \sqrt{\frac{(\chi_T - \chi_S)^2}{4} - \left(\chi' - \frac{\chi_S + \chi_T}{2}\right)^2} \quad (4)$$

where χ_T is the isothermal susceptibility i.e. the susceptibility in zero frequency, and χ_S is the adiabatic susceptibility i.e. the susceptibility at high frequencies where the magnetization is not zero. The solid lines in Fig. 8 represent the simulation semicircles according to Eq. (4) (the respective χ_T and χ_S values at the indicated temperatures are listed in Table S1). The overall magnetic behavior of **2** is similar with that of congener Cu^{II}-Tb^{III} complexes of various topologies and nuclearities which exhibit single-molecule magnet characteristics [33,46b,49–53].

4. Concluding comments

The combination of a Schiff base ligand which contains a coordination pocket of $O_{phenoxo}/N_{imino}$ donor atoms and O_{alkoxo} pentant groups with $Cu(O_2CMe)_2{\cdot}H_2O$ and $Ln(NO_3)_3{\cdot}6H_2O$ (Ln = Gd, Tb) afforded two heptanuclear heterometallic complexes $[Cu_5Ln_2(O_2$-

$CMe)_2(NO_3)_4(L)_2(HL)_2]$ (Ln = Gd (**1**), Tb (**2**)) whose magnetic properties depend on the nature of the Ln^{III} ion. The molecular structure of **1** consists of five Cu^{II} and two Gd^{III} ions linked through two L^{3-} and two HL^{2-} ligands, two μ_3-κ^3O:$\kappa O'$ $MeCO_2^-$ ligands and four chelate nitrates. The metal topology is best described as two distorted $\{Cu_3Gd\}$ cubane subunits with a common apex on a Cu^{II} ion. The isomorphous structure of **2** was confirmed by powder XRD measurements. The magnetic susceptibility data for both complexes revealed the presence of dominant ferromagnetic interactions between the metal ions. Magnetization measurements for **1** suggest a ground state of spin $S = 17/2$ which arises considering that the central Cu^{II} ion is antiferromagnetically coupled to the Cu_4Gs_2 moiety. The magnetocaloric effect of **1**, examined by isothermal magnetization studies under $\Delta H = 5$ T, revealed the maximum entropy change of 15.7 J kg^{-1} K^{-1}at 2 K. The significant anisotropy of Tb^{III} resulted in single-molecule magnet behavior for **2** as shown in ac susceptibility measurements. More work is currently underway in our group to prepare and characterize other members of this family of $\{Cu_5Ln_2\}$ complexes by varying the lanthanide ions and the Schiff base ligands in order to gain insight into their magnetic properties.

Acknowledgment

This research is implemented through IKY Scholarships Programme and co-financed by the European Union (European Social Fund – ESF) and Greek national funds through the action entitled "Reinforcement of Postdoctoral Researchers", in the framework of the Operational Programme "Human Resources Development Programme, Education and Lifelong Learning" of the National Strategic Reference Framework (NSRF) 2014–2020».

Appendix A. Supplementary data

CCDC 1833290 contains the supplementary crystallographic data for this paper. These data can be obtained free of charge via http://www.ccdc.cam.ac.uk/conts/retrieving.html, or from the Cambridge Crystallographic Data Centre, 12 Union Road, Cambridge CB2 1EZ, UK; fax: (+44) 1223-336-033; or e-mail: deposit@ccdc.cam.ac.uk. Supplementary data associated with this article can be found, in the online version, at https://doi.org/10.1016/j.poly.2018.05.003.

References

[1] Molecular Nanomagnets and Related Phenomena, Ed. S. Gao, Struct. Bond. 164, 2015.
[2] F. Torres, J.M. Hernández, X. Bohigas, J. Tejada, Appl. Phys. Lett. 77 (2000) 3248.
[3] G. Lorusso, J.W. Sharples, E. Palacios, O. Roubeau, E.K. Brechin, R. Sessoli, A. Rossin, F. Tuna, E.J.L. McInnes, D. Collison, M. Evangelisti, Adv. Mater. 25 (2013) 4653.
[4] J.-L. Liu, Y.-C. Chen, F.-S. Guo, M.-L. Tong, Coord. Chem. Rev. 281 (2014) 26.
[5] S. Zhang, P. Cheng, Chem. Rec. 16 (2016) 2077.
[6] P. Richardson, D.I. Alexandropoulos, L. Cuhna-Silva, G. Lorusso, M. Evangelisti, J. Tang, T.C. Stamatatos, Inorg. Chem. Front. 2 (2015) 945.
[7] D.I. Alexandropoulos, K.M. Poole, L. Cuhna-Silva, J.A. Sheikh, W. Wernsdorfer, G. Christou, T.C. Stamatatos, Chem. Commun. 53 (2017) 4266.
[8] D.I. Alexandropoulos, L. Cuhna-Silva, G. Lorusso, M. Evangelisti, J. Tang, T.C. Stamatatos, Chem. Commun. 52 (2016) 1693.
[9] K. Liu, W. Shi, P. Cheng, Coord. Chem. Rev. 289–290 (2015) 74.
[10] H.L.C. Feltham, S. Brooker, Coord. Chem. Rev. 276 (2014) 1.
[11] P.A. Vigato, V. Peruzzo, S. Tamburini, Coord. Chem. Rev. 256 (2012) 953.
[12] R. Sessoli, A.K. Powell, Coord. Chem. Rev. 253 (2009) 2328.
[13] H. Ke, L. Zhao, Y. Guo, J. Tang, Dalton Trans. 41 (2012) 2314.
[14] S. Nayak, O. Roubeau, S.J. Teat, C.M. Beavers, P. Gamez, J. Reedijk, Inorg. Chem. 49 (2010) 216.
[15] A. Bhunia, M.T. Gamer, L. Ungur, L.F. Chibotaru, A.K. Powell, Y. Lan, P.W. Roesky, F. Menges, C. Riehn, G. Niedner-Schatteburg, Inorg. Chem. 51 (2012) 9589.
[16] A. Bhunia, M. Yadav, Y. Lan, A.K. Powell, F. Menges, C. Riehn, G. Niedner-Schatteburg, P.P. Jana, R. Riedel, K. Harms, S. Dehnen, P.W. Roesky, Dalton Trans. 42 (2013) 2445.
[17] G. Wu, I.J. Hewitt, S. Mameri, Y. Lan, R. Clérac, C.E. Anson, S. Qiu, A.K. Powell, Inorg. Chem. 46 (2007) 7229.
[18] Y. Zheng, X.-J. Kong, L.-S. Long, R.-B. Huang, L.-S. Zheng, Dalton Trans. 40 (2011) 4035.
[19] T. Shiga, T. Onuki, T. Matsumoto, H. Nojiri, G.N. Newton, N. Hoshino, H. Oshio, Chem. Commun. 45 (2009) 3568.
[20] L. Zhao, J. Wu, S. Xue, J. Tang, Chem. Asian J. 7 (2012) 2419.
[21] J.-L. Liu, F.-S. Guo, Z.-S. Meng, Y.-Z. Zheng, J.-D. Leng, M.-L. Tong, L. Ungur, L.F. Chibotaru, K.J. Heroux, D.N. Hendrickson, Chem. Sci. 2 (2011) 1268.
[22] B. Liu, Q. Liu, H. Xiao, W. Zhang, R. Tao, Dalton Trans. 42 (2013) 5047.
[23] R. Koner, H.-H. Lin, H.-H. Wei, S. Mohanta, Inorg. Chem. 44 (2005) 3524.
[24] J.-P. Costes, B. Donnadieu, R. Gheorghe, G. Novitchi, J.-P. Tuchagues, L. Vendier, Eur. J. Inorg. Chem. (2008) 5235.
[25] M. Towatari, K. Nishi, T. Fujinami, N. Matsumoto, Y. Sunatsuki, M. Kojima, N. Mochida, T. Ishida, N. Re, J. Mrozinski, Inorg. Chem. 52 (2013) 6160.
[26] R. Gheorghe, M. Andruh, J.-P. Costes, B. Donnadieu, M. Schmidtmann, A. Müller, Inorg. Chim. Acta 360 (2007) 4044.
[27] L. Xu, Q. Zhang, G. Hou, P. Chen, G. Li, D.M. Pajerowski, C.L. Dennis, Polyhedron 52 (2013) 91.
[28] J.-P. Costes, S. Shova, W. Wernsdorfer, Dalton Trans. 37 (2008) 1843.
[29] J.-P. Costes, M. Auchel, F. Dahan, V. Peyrou, S. Shova, W. Wernsdorfer, Inorg. Chem. 45 (2006) 1924.
[30] T. Hamamatsu, K. Yabe, M. Towatari, S. Osa, N. Matsumoto, N. Re, A. Pochaba, J. Mrozinski, J.-L. Gallani, A. Barla, P. Imperia, C. Paulsen, J.-P. Kappler, Inorg. Chem. 46 (2007) 4458.
[31] S. Osa, T. Kido, N. Matsumoto, N. Re, A. Pochaba, J. Mrozinski, J. Am. Chem. Soc. 126 (2004) 420.
[32] V. Chandrasekhar, A. Dey, S. Das, M. Rouzières, R. Clérac, Inorg. Chem. 52 (2013) 2588.
[33] L. Jiang, B. Liu, H.-W. Zhao, J.-L. Tian, X. Liu, S.-P. Yan, CrystEngComm 17 (2017) 1816.
[34] A. Dey, S. Das, S. Kundu, A. Mondal, M. Rouzières, C. Mathonière, R. Clérac, R. Suriya Narayanan, V. Chandrasekhar, Inorg. Chem. 56 (2017) 14612.
[35] Rigaku/MSC, CrystalClear, Rigaku/MSC Inc., The Woodlands, Texas, USA, 2005.
[36] (a) G.M. Sheldrick, Acta Crystallogr., Sect. A64 (2008) 112;
(b) G.M. Sheldrick, Acta Crystallogr., Sect. C71 (2015) 3.
[37] DIAMOND – Crystal and Molecular Structure Visualization, Ver. 3.1, Crystal Impact, Rathausgasse 30, 53111, Bonn, Germany.
[38] K. Mounika, B. Anupama, J. Pragathi, C. Gyanakumari, J. Sci. Res. 2 (2010) 513.
[39] L.J. Bellamy, The Infra-red Spectra of Complex Molecules, Chapman and Hall, London, 1975.
[40] K. Nakamoto, Infrared and Raman Spectra of Inorganic and Coordination Compounds, 4th ed., Wiley, New York, 1986.
[41] M. Llunell, D. Casanova, J. Girera, P. Alemany and S. Alvarez, SHAPE, version 2.0, Barcelona, Spain, 2010.
[42] F. Torres, X. Bohigas, J.M. Hernández, J. Tejada, J. Phys.: Condens. Matter 15 (2003) L119.
[43] (a) S.K. Langley, N.F. Chilton, B. Moubaraki, T. Hooper, E.K. Brechin, M. Evangelisti, K.S. Murray, Chem. Sci. 2 (2011) 1166;
(b) T.N. Hooper, J. Schnack, S. Piligkos, M. Evangelisti, E.K. Brechin, Angew. Chem. Int. Ed. 51 (2012) 4633.
[44] (a) J.-D. Leng, J.-L. Liu, M.-L. Tong, Chem. Commun. 48 (2012) 5286;
(b) J.-L. Liu, Y.-C. Chen, Q.-W. Li, S. Gomez-Coca, D. Aravena, E. Ruiz, W.-Q. Lin, J.-D. Leng, M.-L. Tong, Chem. Commun. 49 (2013) 6549;
(c) J.-L. Liu, W.-Q. Lin, Y.-C. Chen, S. Gómez-Coca, D. Aravena, E. Ruiz, J.-D. Leng, M.-L. Tong, Chem. Eur. J. 19 (2013) 17567.
[45] (a) H. Zhang, G.-L. Zhuang, X.-J. Kong, Y.-P. Ren, L.-S. Long, R.-B. Huang, L.-S. Zheng, Cryst. Growth Des. 13 (2013) 2493;
(b) D. Dermitzaki, G. Lorusso, C.P. Raptopoulou, V. Psycharis, A. Escuer, M. Evangelisti, S.P. Perlepes, T.C. Stamatatos, Inorg. Chem. 52 (2013) 10235;
(c) P. Richardson, D.I. Alexandropoulos, L. Cunha-Silva, G. Lorusso, M. Evangelisti, J. Tang, T.C. Stamatatos, Inorg. Chem. Front. 2 (2015) 945.
[46] (a) T.N. Hooper, R. Inglis, M.A. Palacios, G.S. Nichol, M.B. Pitak, S.J. Coles, G. Lorusso, M. Evangelisti, E.K. Brechin, Chem. Commun. 50 (2014) 3498;
(b) S. Xue, Y.-N. Guo, L. Zhao, H. Zhang, J. Tang, Inorg. Chem. 53 (2014) 8165.
[47] T. Rajeshkumar, H.V. Annadat, M. Evangelisti, S.K. Langley, N.F. Chilton, K.S. Murray, G. Rajaraman, Inorg. Chem. 54 (2015) 1661.
[48] J. Bartolome, G. Filoti, V. Kuncser, G. Schinteie, V. Mereacre, C.E. Anson, A.K. Powell, D. Prodius, C. Turta, Phys. Rev. B 80 (2009) 014430.
[49] A. Dey, S. Das, S. Kundu, A. Mondal, M. Rouzières, C. Mathonière, R. Clérac, R. Suriya Narayanan, V. Chandrasekhar, Inorg. Chem. 56 (2017) 14612.
[50] P. Mahapatra, S. Ghosh, N. Koizumi, T. Kanetomo, T. Ishida, M.G.B. Drew, A. Ghosh, Dalton Trans. 46 (2017) 12095.
[51] X.-C. Huang, X.-H. Zhao, D. Shao, X.-Y. Wang, Dalton Trans. 46 (2017) 7232.
[52] Y.-A. Liu, C.-Y. Wang, M. Zhang, X.-Q. Song, Polyhedron 127 (2017) 278.
[53] J. Zhang, C. Li, J. Wang, M. Zhu, L. Li, Eur. J. Inorg. Chem. (2016) 1383.